caused by the small $\Delta\tilde{n}$ ($1–2 \times 10^{-3}$) and the reduced irregularity in the stripe. The full beam angles at the half power parallel ($\theta\|$) and perpendicular ($\theta\perp$) to the junction plane are 11° and 34°, respectively.

Fig. 4 shows the plots of the spot width of the near-field patterns at 3 mW. The close circles and the open rectangles denote the full width at $1/e^2$ power on the near-field patterns perpendicular and parallel to the junction plane, respectively. The astigmatic distance (ΔZ) which shows the difference of the beam waist position between parallel and perpendicular, is less than 1 μm. This must be attributed to the reduction of the absorption loss outside the active region.

Fig. 5 shows the CW aging test results of the lasers under 60°C, 3 mW conditions. The typical operating currents of the lasers are 27–30 mA. The lasers have been operating with little degradation for over 1000 h.

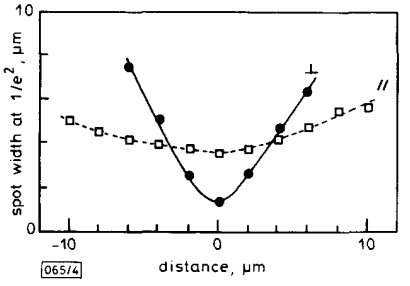

Fig. 4 *Spot width of near-field patterns, parallel and perpendicular to junction plane*

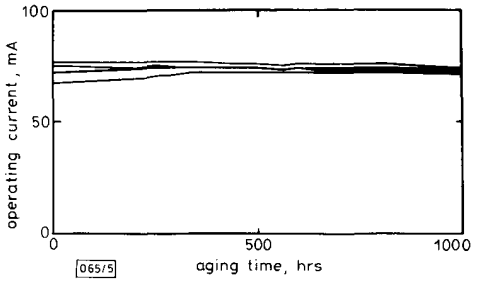

Fig. 5 *CW aging test result at 60°C and 3 mW*

The Zn diffusion stripe laser is fabricated by the MOCVD and the open-tube, two-step, solid phase diffusion technique. The internal loss is reduced by these techniques. The low threshold current and the fundamental transverse mode operation are realised in the wavelength of 780 nm. This laser is expected to be useful for handy type optical systems and OEICs.

A. SHIMA
T. KAMIZATO
A. TAKAMI
S. KARAKIDA
K. ISSHIKI
H. MATSUBARA

Optoelectronic and Microwave Devices R&D Laboratory
Mitsubishi Electric Corporation
4-1 Mizuhara, Itami, Hyogo 664, Japan

29th March 1990

References

1 NOBUHARA, H., SANADA, T., KUNO, M., MAKIUCHI, M., FUJII, T., and WADA, W.: 'OEIC transmitter fabricated by planar integration process'. Extended Abstract 18th Conf. Solid State Devices and Materials, Tokyo, 1986, pp. 185–188

2 UENO, M., and YONEZU, H.: 'Stable transverse mode oscillation in planar stripe laser with deep Zn diffusion', *IEEE J. Quantum Electron.*, 1979, **QE-15**, pp. 1189–1196

3 HAHAMITSU, K., OHSAKA, S., YOSHIDA, K., NISHI, H., HORI, K., and TAKUSAGAWA, T.: 'Semicylindrical Zn-diffused stripe GaAlAs laser diodes with very low threshold currents', *Electron. Lett.*, 1982, **18**, pp. 853–855

4 MATSUO, N., KAWAGUCHI, M., AIDA, H., MATSUMOTO, N., IKEGAMI, Y., and KASHIWA, S.: 'GaAs/GaAlAs DDS lasers fabricated by MOCVD and solid to solid diffusion'. Extended Abstracts 48th Autumn Meeting of Japan Society of Applied Physics, Nagoya, October, 1987, p. 737 (18a-ZR-1)

5 SUSAKI, W., and TAKAMIYA, S.: 'Visible semiconductor laser', *Jpn. J. Appl. Phys.*, 1981, **20**, pp. 205–210

6 NAMIZAKI, H., KUMABE, H., and SUSAKI, W.: 'Spontaneous emission behavior in AlGaAs TJS lasers', *IEEE J. Quantum Electron.*, 1981, **QE-17**, pp. 799–803

7 SELL, D. D., CASEY, H. C., JUN., and WECHT, W.: 'Concentration dependence of the refractive index for *n*- and *p*-type GaAs between 1·2 and 1·8 eV eV', *J. Appl. Phys.*, 1974, **45**, pp. 2650–2657

FUNDAMENTAL LIMITATION ON LARGE-SIGNAL MODULATION OF SEMICONDUCTOR LASERS AND ITS IMPLICATIONS FOR LIGHTWAVE TRANSMISSION

Indexing terms: Lasers and laser applications, Semiconductor lasers, Modulation

The performance of single-mode semiconductor lasers under large signal modulation is found to be limited by intraband gain saturation occurring when the on-state output power becomes comparable to the saturation level. The main effect of intraband gain saturation is to increase the fall time associated with the optical pulse. At high bit rates the pulse stretches over several neighbouring bits, thereby affecting the system performance. In the case of 1·55 μm InGaAsP lasers operating at bit rates ~10 Gbit/s intraband gain saturation limits the average power in the range ~10–20 mW for an acceptable system performance.

The development of high-performance optical communication systems is of continued practical interest. Data transmission at 10 Gbit/s over 100 km of fibre length has been demonstrated by using a 1·5 μm distributed feedback (DFB) laser together with dispersion-shifted fibre.[1] The optical power launched into the fibre is typically ~1 mW in most of such laboratory demonstrations. In principle, the transmission distance can be increased further if more power is launched into the fibre by using high-power DFB lasers (as long as stimulated Brillouin scattering is not a limiting factor). In practice, one should inquire whether a fundamental phenomenon exists that would limit the high-speed modulation of high-power DFB lasers. This letter shows that intraband gain saturation is such a limiting phenomenon. When the on-state power of the modulated signal becomes comparable to a critical power level set by the intraband relaxation time, the rise and fall times of the optical pulse are found to increase considerably. Since a considerable portion of the pulse energy lies outside the allocated bit slot, intersymbol interference is likely to limit the system performance.

Intraband gain saturation manifests itself through a reduction in the optical gain at high power levels. By using the density-matrix formalism for a single-mode DFB laser, the optical gain is found to be[2]

$$g(n, S) = \frac{a(n - n_0)}{\sqrt{(1 + S/S_{sat})}} \tag{1}$$

where n is the carrier density, S is the photon density, a is the differential gain coefficient, n_0 is the transparency value of the carrier density, and the saturation photon density, S_{sat}, is given by

$$S_{sat} = \frac{\varepsilon_0 \bar{n} n_g \hbar}{\mu^2 \omega_0 \tau_{in}(\tau_c + \tau_v)} \tag{2}$$

where $\bar{n}$ is the mode index, n_g is the group index, μ is the dipole moment, ω_0 is the mode frequency, τ_{in} is the intraband

polarisation relaxation time, and τ_c and τ_v are the corresponding population relaxation times for the conduction and valence bands, respectively. Intraband gain saturation does not occur if the induced polarisation relaxes instantaneously ($\tau_{in} = 0$). Typically $\tau_{in} \simeq 100$ fs for InGaAsP semiconductor lasers.

The large-signal modulation response is obtained by solving the rate equation written in the form[3,4]

$$\frac{dS}{dt} = \left(\Gamma v_g g - \frac{1}{\tau_p}\right)S + \frac{\Gamma n_{sp}}{V\tau_p} \tag{3}$$

$$\frac{dn}{dt} = \frac{I}{qV} - \frac{n}{\tau_n} - v_g g S \tag{4}$$

where Γ is the confinement factor, v_g is the group velocity, n_{sp} is the spontaneous emission factor, V is the active volume, τ_p and τ_n are the photon and carrier lifetimes, and the injected current, I, is given by

$$I(t) = I_b + I_p f(t) \tag{5}$$

where I_b is the bias current, I_p is the peak value of the modulation current, and $f(t)$ is the pulse-shape function. To represent a nearly rectangular current pulse, we choose a super-Gaussian form for $f(t)$ and take

$$f(t) = \exp\left[-\left(\frac{2t}{T_b}\right)^{T_b/T_r}\right] \tag{6}$$

where $T_b = 1/B$ is the bit duration at the bit rate, B, and T_r is the rise time. We use $T_r = 0{\cdot}2T_b$ as a representative value.

The rate eqns. 3 and 4 are solved numerically for a 1·55 μm InGaAsP laser with active-layer dimensions of 250 × 2 × 0·2 μm.[3] The other parameters are $a = 2{\cdot}5 \times 10^{-16}$ cm^2, $n_0 = 1 \times 10^{18}$ cm^{-3}, $\Gamma = 0{\cdot}4$, $\bar{n} = 3{\cdot}3$, $n_g = 3{\cdot}4$, $n_{sp} = 1{\cdot}7$, and $\tau_p = 1{\cdot}5$ ps. The carrier lifetime τ_n was allowed to vary with n to include the effect of Auger recombination and had a value of 2·12 ns at the laser threshold. The laser is biased at threshold ($I_b = I_{th}$) and modulated 10 times above threshold ($I_p = 10I_{th}$). The effect of intraband gain saturation is studied by varying the saturation output power P_{sat}, related linearly to S_{sat}, over the range 20–60 mW. The saturation photon density is estimated to be $S_{sat} \sim 3 \times 10^{16}$ cm^{-3}. However, P_{sat} depends on what fraction of intracavity photons escapes from the output facet and may vary with the DFB laser parameters such as the facet reflectivity and the coupling coefficient.

Consider first the case of a DFB laser modulated at 5 Gbit/s. Fig. 1 shows optical pulse shapes for three values of P_{sat}. The current pulse is also shown for comparison. For $P_{sat} = 60$ mW, the optical pulse exhibits a relaxation-oscillation spike as relaxation oscillations are not heavily damped for such a large saturation power. The amplitude of the spike decreases with a decrease in P_{sat}; the spike disappears altogether for $P_{sat} = 20$ mW. The most noteworthy feature of Fig. 1 is the appearance of a long tail on the trailing side of the optical pulse with a decrease in P_{sat}. The tail is indicative of an increase in the fall time occurring because of intraband gain saturation. The situation worsens at high bit rates since the fall time is nearly independent of the bit rate. Fig. 2 shows the optical pulse shapes for the same device parameters except for the bit rate that is doubled to $B = 10$ Gbit/s. For $P_{sat} = 20$ mW, the pulse tail is so long that it extends into the two neighbouring bit slots.

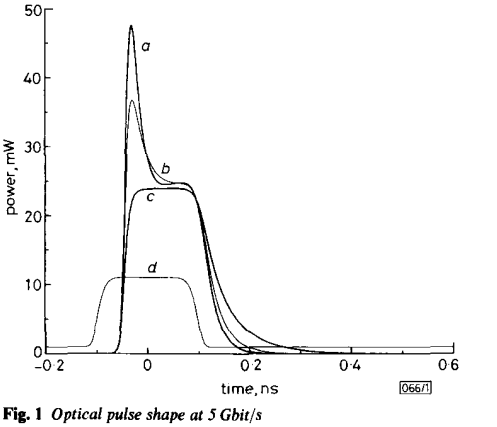

Fig. 1 *Optical pulse shape at 5 Gbit/s*
a $P_{sat} = 60$ mW
b $P_{sat} = 40$ mW
c $P_{sat} = 20$ mW
d Current pulse

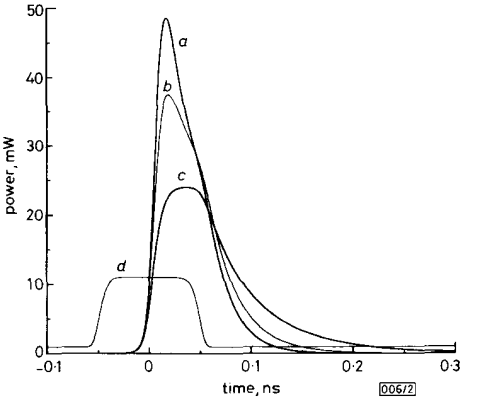

Fig. 2 *Optical pulse shape at 10 Gbit/s*
a $P_{sat} = 60$ mW
b $P_{sat} = 40$ mW
c $P_{sat} = 20$ mW
d Current pulse

What are the implications of intraband gain saturation for the performance of high-speed lightwave systems? The long tail on the trailing side of the optical pulse would lead to unacceptable intersymbol interference and bit-pattern-dependent effects that must be avoided in a realistic lightwave system. This would limit the on-state optical power, P_{on}, below the saturation level. Our numerical results suggest that intraband gain saturation would not limit the performance of a 10 Gbit/s lightwave system as long as $P_{on} < P_{sat}/2$. The saturation output power P_{sat} is related to S_{sat} by the relation $P_{sat} = \eta_{out}\tau_m v_g \hbar\omega_0 S_{sat}$, where η_{out} is the differential quantum efficiency of the output facet and σ_m is the cross-section area of the optical mode. By using S_{sat} from eqn. 2, P_{sat} is given by

$$P_{sat} = \frac{\varepsilon_0 c\hbar^2 \bar{n}\eta_{out}\sigma_m}{\mu^2\tau_{in}(\tau_c + \tau_v)} \tag{7}$$

For a specific 1·55 μm InGaAsP laser P_{sat} is estimated to be 30 mW by using the parameter values $\bar{n} = 3{\cdot}3$, $\mu = 9 \times 10^{-29}$ mC, $\tau_{in} = 0{\cdot}1$ ps, $\tau_c = 0{\cdot}3$ ps, $\tau_v = 0{\cdot}07$ ps, $\sigma_m = 1\,\mu$m^2, and $\eta_{out} = 0{\cdot}1$. The on-state modulated power P_{on} for this laser is limited to about 15 mW. However, P_{on} can be increased by a factor of two or more by designing the laser so that η_{out} and σ_m are relatively large. The average power ($P_{av} = P_{on}/2$) is expected to be limited in the range 10–20 mW in most cases of practical interest.

In conclusion, intraband gain saturation is found to limit the performance of single-mode semiconductor lasers under large-signal modulation. The main effect of intraband gain saturation is to increase the fall time associated with the optical pulse when the on-state output power becomes comparable to the intraband saturation level. If the fall time exceeds the bit duration considerably, the optical pulse develops a long tail that stretches over several neighbouring bits. The on-state output power should be a fraction of the intraband saturation power for an acceptable performance of the optical communication systems. In the case of 1·55 μm InGaAsP lasers operating at high bit rates (~10 Gbit/s) intraband gain saturation limits the average power in the range

~10–20 mW. The limiting average power may be lower for quantum-well lasers as the saturation power is reduced because of quantum confinement.[5]

The research is supported by the US Army Research Office and the Joint Services Optics Program.

G. P. AGRAWAL

The Institute of Optics
University of Rochester
Rochester, NY 14627, USA

29th March 1990

References

1 FUJITA, S., KITAMURA, M., TORIKAI, T., HENMI, N., YAMADA, H., SUZAKI, T., TAKANO, I., and SHIKADA, M.: '10 Gbit/s, 100 km optical fibre transmission experiment using high-speed MQW DFB-LD and back-illuminated GaInAs APD', *Electron. Lett.*, 1989, **25**, pp. 702–703

2 AGRAWAL, G. P.: 'Spectral hole-burning and gain saturation in semiconductor lasers: Strong-signal theory', *J. Appl. Phys.*, 1988, **63**, pp. 1232–1234

3 TUCKER, R. S.: 'High-speed modulation of semiconductor lasers', *J. Lightwave Technol.*, 1985, **LT-3**, pp. 1180–1192

4 AGRAWAL, G. P., and DUTTA, N. K.: 'Long-wavelength semiconductor lasers' (Van Nostrand Reinhold, New York, 1986)

5 ARAKAWA, Y., and TAKAHASHI, T.: 'Effect of nonlinear gain on modulation dynamics in quantum-well lasers', *Electron. Lett.*, 1989, **25**, pp. 169–170

COMBINED AMPLITUDE AND POLARISATION SHIFT KEYING OPTICAL COHERENT MODULATION

Indexing terms: Optical communications, Polarisation, Optical modulation

The letter proposes and analyses two coherent transmission schemes using combined amplitude and polarisation shift keying (CAPSK). The bit-error-rate results (with respect to shot and Gaussian receiver noise) show a performance very close to that of the best performing schemes known so far.

Introduction: The state of polarisation (SOP) of a fully polarised lightwave provides a new modulation parameter that can be exploited for digital transmission in optical fibre systems. A number of theoretical papers have been presented on this matter during the last three years, together with a few experimental demonstrations.[1,2]

In two previous letters[1,2] and papers[3,4] we have presented the theoretical analysis of detection, noise statistics and maximum likelihood (ML) decision rules for this class of systems, called POLSK (polarisation shift keying). We have also carried out the exact (for shot and Gaussian receiver noise) performance analysis of eight different binary and multilevel system configurations.

In this letter, we present original results on two multilevel schemes that combine polarisation and amplitude modulation. We called them combined amplitude and polarisation shift keying systems (CAPSK).

To analyse these systems, it is necessary to use most of the previously developed theoretical results on multilevel POLSK constellations, treated in the Stokes space representation. These topics have been fully presented in previous work[3,4] and we shall not discuss them here.

The bit-error-rate results presented in this letter can be considered exact for shot and Gaussian receiver noise. A few comments on phase noise are also given.

CAPSK constellations: Paralleling what is done in QAM systems to improve on PSK, we try to exploit the third degree of freedom of the Stokes space to improve on M-POLSK systems for a given M.

We propose and analyse two CAPSK systems, whose signal constellations are the superposition, at different power levels, of two constellations of equipower signals. Since in the Stokes space the distance from the origin of a point representing a certain SOP is linearly proportional to the power of the carrier, the resulting constellation will be made up of two equipower constellations lying over Poincaré spheres with different radii.

We use signal constellations derived from the vertices of regular polyhedra inscribed into a Poincaré sphere. In detail, we propose a 16-CAPSK, which combines a 4-POLSK (tetrahedron) and a 12-POLSK (icosahedron) constellation, and a 32-CAPSK scheme (12-POLSK (icosahedron) + 20-POLSK (dodecahedron)).

To generate these signals, it is sufficient to use the SOP modulator[3] together with an amplitude modulator, placed either at the input or at the output of the modulator itself.

Error probability evaluation for CAPSK constellations: The performance evaluation of M-POLSK systems based on the separate equipower constellations addressed here can be found in Reference 1 for 4-POLSK (tetrahedron), and in Reference 3 for 12-POLSK (icosahedron) and 20-POLSK (dodecahedron) schemes. The CAPSK solutions that we present here are conceived so that the equipower constellation, which is automatically more noise-tolerant, is transmitted at a lower power level than the less noise-tolerant constellation.

Therefore, for instance, the 16-CAPSK is made of two spherical 'shells': on the internal one (lower power) we place a 4-POLSK (tetrahedron) constellation, and on the external shell (higher power) we put a 12-POLSK (icosahedron) constellation. Between these two shells, we ideally place a sphere whose radius is intermediate between those of the shells. This sphere behaves as a 'threshold': if a point below the threshold is received, the decision device assumes that a signal belonging to the lower shell was transmitted and uses the 4-POLSK tetrahedron ML decision regions to decide; otherwise, it uses the 12-POLSK icosahedron ones. Those individual decision regions were determined in an optimal way in References 2 and 3. The same strategy is used for the 32-CAPSK solution, made up with the 12-POLSK icosahedron on the inner sphere plus the 20-POLSK dodecahedron on the outer one.

Though not necessarily optimum, this partitioning of the Stokes space permits a much easier implementation and yields good performance results.

By a relatively straightforward procedure, it can be shown that the resulting symbol error probability is

$$P(E) = P(S_i \in \mathscr{L})[p_{\mathscr{L}} + P(|S_N| > \rho_s | S_i \in \mathscr{L})] + P(S_i \in \mathscr{H})[p_{\mathscr{H}} + P(|S_N| < \rho_s | S_i \in \mathscr{H})] \quad (1)$$

where ρ_s is the radius of the sphere that acts as a threshold, $\mathscr{L}(\mathscr{H})$ is the set of signal points belong to the lower (higher) constellation and $p_{\mathscr{L}}(p_{\mathscr{H}})$ is the error probability of the lower (higher) constellation alone, evaluated at the signal/noise ratio of its own signals (lower SNR for the lower constellation). Using the toal cumulative distribution of the ρ co-ordinate[1,4] of the received point S_n, we have

$$P(|S_N| > \rho_s | S_i \in \mathscr{L}) = Q_2[\sqrt{(2\eta_{\mathscr{L}})}, \sqrt{(\rho_s)}]$$

$$P(|S_N| < \rho_s | S_i \in \mathscr{H}) = 1 - Q_2[\sqrt{(2\eta_{\mathscr{H}})}, \sqrt{(\rho_s)}]$$

where $\eta_{\mathscr{L}}$, $\eta_{\mathscr{H}}$ are the SNRs for signal points belonging to the inner and outer shells, respectively, and Q_2 is a generalised Marcum function of order two.

To be precise, the RHS of eqn. 1 represents an upper bound to $P(E)$. However, it can be shown that the error involved is less than $2[P(E)]^2$, so that at $P(E) = 10^{-9}$ the error is below 2×10^{-17}. Therefore, with respect to all practical uses, it can be considered exact.

To compute the actual $P(E)$, we need to specify two parameters: the power ratio between the upper and lower shells, and the threshold level ρ_s. In our calculations we have optimised these parameters. Thus, for a given pair of constellations, we were able to find the best $P(E)$ performance.